Journal of Marine Science and Application (2026) 25: 175-196
https://doi.org/10.1007/s11804-025-00648-x

RESEARCH ARTICLE

Optimized Skimmer Design for Enhanced Oil Spill Recovery and Marine Environmental Protection: Addressing Key Challenges in Oceanic Pollution Control

Alireza Zahedi[1] and Behzad Kanani[1]

Received: 07 October 2024 / Accepted: 18 November 2024

Abstract

Environmental pollution, energy consumption, and greenhouse gas emissions are critical global issues. To address these challenges, optimizing skimmer coatings is a major step in commercializing cleaning oil stains. This research presents a novel approach to creating and refining oil-absorbent coatings, introducing a unique oil spill removal skimmer enhanced with a super hydrophobic polyaniline (PANI) nanofiber coating. The goal of this study was to improve oil absorption performance, increase the contact angle, lower drag, reduce energy consumption, achieve high desirability, and lower production costs. PANI treated with hydrochloric acid was a key focus as it resulted in higher porosity and smaller pore diameters, providing a larger surface area, which are crucial factors for boosting oil absorption and minimizing drag. To optimize optimal nanofiber morphology, PANI synthesized with methanesulfonic acid was first dedoped and then redoped with hydrochloric acid. After optimization, the most effective skimmer coating was achieved using a formulation consisting of 0.1% PANI, an ammonium persulfate/aniline ratio of 0.4, and an acid/aniline ratio of 9.689, along with redoped PANI nanofibers. The optimized skimmer exhibited a remarkable contact angle of 177.477°. The coating achieved drag reduction of 32%, oil absorption of 88.725%, a cost of $1.710, and a desirability rating of 78.5%. In this study, an optimized skimmer coat containing super hydrophobic coat–PANI nanofibers was fabricated. By enhancing contact angle and reducing drag, these coatings increased the skimmer performance by improving oil absorption and reducing fuel consumption.

Keywords Nanofiber-based skimmer; Oil absorption; Drag reduction; Polyaniline nanofiber; Superhydrophobic; Oil spill removal

1 Introduction

Over the past decades, the rise in oil exploration and production has resulted in numerous environmental challenges. Each year, millions of tons of petroleum products are transported across global open waters, leading to frequent oil spills and significant ecological harm (Abidli et al., 2020; Singh and Jelinek, 2020). Oil residues undergo gradual physical and chemical changes over time. These changes include spreading across water surfaces, dissolving into the water, forming oil-water emulsions, evaporating, breaking down under sunlight through photolysis, and gradually decomposing. These processes can significantly impact the water's properties, such as its viscosity, density, and surface tension.

Given the potential long-term effects of hazardous water-soluble, light hydrocarbons (Kukkar et al., 2020) on both aquatic organisms and humans, the immediate removal of oil spills is essential. Various methods have been implemented to address this issue, including mechanical, chemical, and biological approaches (Singh and Jelinek, 2020). The choice of the optimal method relies on factors such as the size and location of the oil spill, the type of oil involved, and the regional climate. External elements such as wave activity and weather conditions can affect oil evaporation, diffusion, and biological breakdown, potentially leading to the spread of oil slicks (Kukkar et al., 2020). Nevertheless, on a larger scale, physical methods such as booms, skimmers, absorption, and in situ burning are widely used for cleaning oil spills. Despite their popularity, these methods face several drawbacks. These are often costly, inefficient in separation, slow in processing, and may yield impure reclaimed water or oil. Many of these tools are also non-

Article Highlights

- Development of superhydrophobic coatings with polyaniline nanofibers, achieving a contact angle of 177.5° and enhanced oil absorption performance.
- Superhydrophobic coatings with modified polyaniline nanofibers reduced drag force by 32%, improving energy efficiency and lowering operational costs.
- Providing an affordable and efficient approach for managing oil spills, reducing production costs to $1.71 while achieving an oil absorption rate of 88.7%.

✉ Alireza Zahedi
zahediar@iust.ac.ir

[1] School of Advanced Technologies, Iran University of Science and Technology, Tehran 13114-16846, Iran

biodegradable, and their efficacy and suitability depend on various factors, such as the viscosity of the spilled oil, prevailing climate conditions, and environmental conditions. Among physical methods, surface absorption methods are particularly common. These involve tools such as skimmers, oil-absorbing foams, and different nanofibers.

Skimmers are mechanical devices designed to collect oil pollution from the water surface. They perform optimally in clean and calm waters, but their efficiency diminishes in the presence of impurities or ice fragments in the water (Abidli et al., 2020). Moreover, when the wind blows toward the skimmer, it helps accumulate more oily substances. The thickness of the oil layer on the water surface significantly impacts absorption effectiveness, with an optimal thickness improving oil extraction. Multiple skimmer varieties are accessible, including oleophilic, weir, elevating, submersion, suction/vacuum, and vortex/centrifugal methods (Sarbatly et al., 2016). Skimmers rely on absorbent materials to collect and convert the petroleum mixture into a semisolid or solid phase. For an absorbent to be effective in oil skimmers, it must have suitable hydrophobic−oleophilic properties, a high absorption capacity, a high absorption rate, and acceptable flotation. Materials used as absorbents include natural organic materials, natural inorganic materials, and synthetically synthesized organic fibers (Yin et al., 2020). Polypropylene fibers are among the most commonly used synthetic fibers. They are easy to produce, possess excellent physical properties, float well, and can absorb various hydrocarbons in oil spill cleanups. However, their low porosity and large diameter solid fibers result in limited oil absorption (OA) capacity (10–30 grams of oil per material). Therefore, researchers should focus on developing improved absorbent foams (Zhu et al., 2011). Polyurethane (PU) has emerged as a promising synthesized absorbent.

PU is a commercially available, three-dimensional porous material widely studied for creating highly hydrophobic absorbents for water and oil separation. However, like other hydrophobic foams, PU foams face a major challenge, namely low mechanical durability under extreme physical and chemical conditions (Baig et al., 2021). This is often attributed to weak adhesion between the porous three-dimensional skeleton of the foam. An innovative way to improve oil stain separation is by adding adsorbent nanofibers. Immersing PU foam in a superhydrophobic (SH) solution has shown promise in producing an absorbent foam with high porosity, enhanced durability, and improved OA capacity (Khodakarami and Bagheri, 2021). Recently, researchers have developed methods to fabricate pure, uniform, and mold-free PU nanofibers with small diameters (<100 nm) in scalable quantities (Hosseini and Mousavi, 2021). Owing to their exceptional physical properties, nanofiber absorbents are effective solutions for OA. These nanofibers have emerged as valuable options for cleaning oil stains owing to their physical and mechanical properties, such as very high specific surface (SS) areas and small pore sizes (Sarbatly et al., 2016; Xiong et al., 2019). The use of various nanofibers in the structure of absorbing foams has been investigated. In this regard, Lü et al. (2016) developed ultrahydrophobic PU foams by coating them with silica/graphene oxide nanohybrids. These modified foams demonstrated excellent potential as adsorbents, quickly absorbing organic solvents and hydrocarbons. To further improve the performance of PU foams and address their limitations in oil spill isolation, incorporating synthesized compounds such as nanomaterials has gained attention. In this context, polyaniline (PANI) with unique features can be used in this field.

PANI is a conductive polymer valued for its impressive properties as an absorbent material. Its effectiveness depends on factors such as its oxidation state and impurities. It stands out for its environmental stability, low-cost synthesis, ease of forming nanostructures, flexible doping mechanism, simple concentration/dilution process, adjustable electrical properties, and physicochemical properties (Mendieta-Rodríguez et al., 2021; Ghorbankhani and Zahedi, 2022). The presence of large amounts of amine groups (NH-) in PANI makes it particularly suitable for removing heavy metals. For example, it has proven effective in adsorbing chromium (VI) ions (Karthik and Meenakshi, 2015). Among various PANI nanostructures, nanofibers have a high potential to increase performance for removing contaminants from water (Ghorbankhani and Zahedi, 2022). PANI nanofibers, with diameters between 50–80 nm, have been successfully used as highly effective adsorbents for removing RB5 from aqueous solutions through the rapid mixing polymerization method (Bhaumik et al., 2016). Furthermore, doped acid purification methods have enhanced the metal ion adsorption capabilities of PANI nanofibers. Such nanofibers doped with phosphoric acid (PH-PANI) performed significantly better at adsorbing Cu^{2+} than those doped with hydrochloric acid. This improvement is attributed to the higher capacity and strong absorption properties provided by phosphoric acid or phosphate groups. PANI nanofibers doped with phosphoric acid have a larger number of sites (increased porosity), offering more trapping sites for aqueous metal cations owing to the hydroxyl functional groups in phosphoric acid (Kim et al., 2017). Ghorbankhani and Zahedi (2022) produced absorbent polyurethane foams containing PANI nanofibers to clean oil stains and separate water by optimizing nanofiber morphology. The best sample of polyurethane foam containing PANI nanofibers was formed with an aniline/ammonium persulfate (APS) molar ratio of 1.43, an aniline/acid ratio of 0.105, and a concentration of 0.433. This foam exhibited an oil sorption coefficient (OSC) of 5.038 at a cost of $1.748. Polyurethane foam containing optimized PANI nanofibers was 69% more efficient than pure commercial polyurethane foams.

Energy consumption during skimmer activity is a critical factor, largely influenced by drag force. Drag resists the movement of objects through fluids (Tian et al., 2022) and is mainly caused by friction, which depends on the surface morphology (Feng et al., 2020). Friction drags cause energy loss, especially in floats (Heo et al., 2021). Reducing the frictional force applied to ships and submarines can reduce fuel consumption, increase the speed of marine vehicles, and lower greenhouse gas emissions. As a result, reducing drag is necessary. An effective and efficient method to reduce drag is the use of SH coatings (SHCs) (Gose et al., 2021). These coatings can significantly reduce the drag applied to floats. SH surfaces are characterized by an extensive contact angle (CA, higher than 150°) and a slight slip angle (lower than 10°), which allow water drops to easily slide off without sticking. Polymeric materials are inherently hydrophobic. The SH surfaces have distinct properties, including oil and water separation, self-cleaning, antifouling, increased heat transfer, and antibacterial and antiwear effects (Liravi et al., 2020).

This study focuses on developing and optimizing oil-absorbent coatings to improve OA performance, enhance the CA, reduce drag reduction (DR), boost overall desirability, and lower costs. For the first time, an SHC was modified with PANI nanofibers and used to separate oil stains and reduce drag simultaneously in the skimmer. Key benefits include SH properties, a high SS area, high porosity, easy synthesis, low price, availability of raw materials, and environmental compatibility. PANI was doped with various compounds, and the structure and morphology of the resulting nanofibers were thoroughly analyzed. Their performance was tested in separating oil stains. The higher-performing sample was then dedoped and redoped for further evaluation. The results showed that increasing the CA, accompanied by reduced drag, significantly lowered the energy required for the process. This, in turn, reduced fuel consumption and greenhouse gas emissions. This is achieved by using a hybrid renewable energy system, which combines the energy from a parabolic solar collector and the heat and water from a solar still desalination unit. This system not only reduces the environmental impact of the process but also significantly cuts production costs. Finally, the structure of a modified coating for skimmers with optimal and economic performance is introduced.

2 Materials and methods

This study utilized library research to select materials that complemented each other and aligned with the primary goal of designing SH OA skimmers modified with PANI nanofibers. Aniline was utilized as the base material for nanofiber synthesis, while APS served as the oxidizing agent. Various catalysts, including methanesulfonic acid (MSA), nitric acid (NA), sulfuric acid (SA), and hydrochloric acid (HCA), were used to produce PANI. Hydroxyl ammonium served as a doping agent. For testing purposes, deionized water was used as the testing medium, while acetone, sourced from Merck, as acted as the the solvent (Germany). Additionally, a light crude oil refinery was prepared from Tehran oil as the target material for absorption experiments.

2.1 Heat and water supply system

This study used a hybrid system combining a parabolic trough collector and a solar still desalination system (Figure 1) designed by Mirnezami et al. (2020) to provide heat and water. The parabolic trough collector used Thermia B heat transfer oil (USA) as its primary operating fluid. MgO nanoparticles (20–30 nm and 99% purity) and multi-walled carbon nanotubes (20 nm, with over 95% purity) made by Pishgaman Nanomaterials Company of Iran were used to prepare nanofluids in oil-based fluid as hybrid nanofluids to increase system efficiency. The two parabolic mirrors had a reflection coefficient of 0.9. An inner copper tube of 2 mm and an outer glass tube with a thickness of 2 mm were used as the absorber tube. The heat and water supply system also incorporated a single-slope solar still desalination component, selected for its capacity to integrate into the hybrid system.

2.2 PANI Preparation

To ensure material purity, aniline was distilled before the synthesis process as its transparent color tends to turn

Figure 1 Hybrid system

dark brown over time due to exposure to light and air, introducing impurities. Therefore, it was subjected to distillation to purify aniline before the synthesis stage. Aniline has a boiling point of 184 °C, but high temperatures could impact its structure. Therefore, it was distilled three times under vacuum conditions at 70 °C and 0.2 atm.

PANI was synthesized using the dialysis tubing method. First, 0.184 g of APS was dissolved in 200 ml of 1 M MSA and subjected to an ultrasonic bath for 30 min to create the oxidant solution. According to findings from Chuah et al. (2016) on the effect of aniline-to-acid ratios on polymerization outcomes, 150 mg of distilled aniline and 3 ml of 1 M acid were gradually added to the oxidant solution over 24 h. This process was carried out at 25 °C using a 3 500 Da dialysis bag.

After polymerization, the product was washed and purified. The solution was placed in 12 000 Da dialysis tubing and immersed in 4 liters of distilled water for 24 h. The pH of the PANI solution was monitored every 24 h, and if not neutral, the process was repeated for another 24 h. This ensured the removal of residual acid and allowed the polymer to settle inside the tubing. Once the pH stabilized at 7, the polymer was collected and dried in a vacuum oven at 60 °C for 8 h, resulting in a water-soluble PANI powder. Three additional types of PANI were synthesized using HCA and NA at a concentration of 0.2 M. The synthesis process followed the same steps as those used for PANI with MSA, utilizing 3 500 Da dialysis tubing with similar washing and drying stages. Three other types of PANI were washed and prepared using HCA, SA, and NA at 0.2 M, following precisely the steps outlined for the synthesis of PANI with MSA by 3 500 Da dialysis tubing with similar washing and drying stages.

2.3 Superhydrophilic color

A commercial SHC was used as the base coating. Specifically, the NANOMYTE SuperCN Plus product, which has a CA of 150°, was used. Scanning electron microscopy (SEM) images of the samples, taken at 50× and 200× magnification, are shown in Figure 2.

2.4 Governing equations

The ASTMF726 standard was used to evaluate the performance of the skimmer as an absorbent. In this context, OSC was utilized, representing a crucial and pragmatic element in assessing the effectiveness of skimmers in absorbing all kinds of possible oil spills. Equation (1) calculates the OSC.

$$\mathrm{OSC} = \left(\frac{G_{\mathrm{OS}} - G_{\mathrm{O}}}{G_{\mathrm{O}} + G_{\mathrm{wu}}} \right) \tag{1}$$

where OSC is expressed in g/g, G_{OS} denotes the weight of the absorbing material after OA (g), and G_{O} represents the original dry absorbent weight (in grams). At the same time, G_{wu} signifies the water weight that the foam absorbs. Equation (2) is as follows:

$$G_{\mathrm{wu}} = \left(\frac{G_{\mathrm{ws}} - G_{\mathrm{O}}}{G_{\mathrm{O}}} \right) \tag{2}$$

where G_{ws} refers to the dry absorbent weight after water absorption. Friction torque was measured using a parallel plate rheometer to investigate the DR performance of the SH surfaces. The DR rate is calculated via Equation (3) (Lv et al., 2021):

$$\text{Drag reduction rate}\,(\%) = \left(1 - \frac{M_1}{M_2}\right) \times 100 \tag{3}$$

where M_1 and M_2 are the friction torques of the coatings with and without SH properties, respectively.

2.5 Design of the experiment

The synthesis of PANI synthesis through polymerization using a semipermeable membrane depends on numerous factors. These include the molarity ratios of monomer to oxidant, oxidant to catalyst, and monomer to catalyst, in addition to the temperature and duration of polymerization. Additionally, various laboratory conditions, such as the polymer-to-foam concentration ratio, foam formation pressure and temperature, and the mixing ratios of different components, are essential for developing PANI nanofiber foams. The main goals of synthesizing these absorbent foams include achieving cost-effectiveness, high absorption efficiency, tailored hydrophobic or hydrophilic properties, and

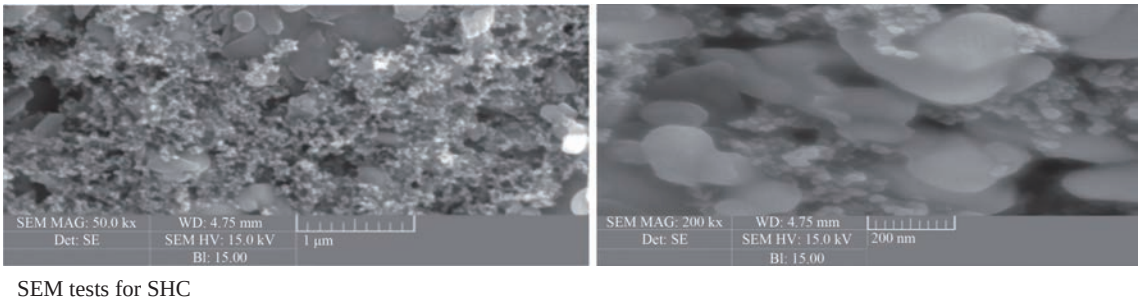

Figure 2 SEM tests for SHC

scalability for industrial applications. To reach these goals, a thorough investigation and optimization of the process using experimental design techniques are crucial. Optimization was performed using test designs and a sensitivity analysis of the effective parameters on the optimized responses via Design Expert 10.

Key factors in the PANI synthesis process include the molarity ratio between aniline and APS and the molarity ratio between aniline and the doped acid. Moreover, PANI concentration within the raw SHCfoam emerged as a crucial factor influencing the absorption rate. Table 1 outlines these critical parameters within the test design.

Table 1 Parameters affecting the polymerization test as a design variable

Design parameter	Reason for selection
Ratio of aniline to APS (Aniline/APS) (mol/mol)	Nanofibers morphology investigation
Ratio of aniline to MSA (Aniline/MSA) (mg/ml)	Simultaneous investigation of nanofiber morphology and cost
PANI concentration in SH foam (PANI concentration) (%)	Investigating the effect on oil stain absorption

The main goal of this research was to achieve the highest rate of crude OA. Consequently, the OSC was identified as one of the key responses. Notably, as the amount of absorbed crude oil increases, the OSC also rises, making it a favorable outcome. Another crucial solution influencing the commercial success of the end product is cost. Reducing the product's final cost is beneficial; however, this goal presents a trade-off with the OSC, as it acts as a constraining factor. Table 2 highlights the selected responses for this study. After identifying the effective design parameters and desired output responses, along with determining appropriate variation ranges, an efficient experimental design can be created to meet the research goals. The variation range of the design parameters is listed in Table 3.

Table 2 Selected response as the dependent variable

Response	Reason for selection
OSC	Examining the effectiveness of the absorbent sample
CA	Investigating the SH property of coatings
Cost	Investigating the commercialization and operability of the absorber

Table 3 Variations in the design parameters

Design variables	Variation range
Aniline/APS	$0.75 \leqslant X \leqslant 2.5$
Aniline/MSA (mg/ml)	$0.029\,4 \leqslant X \leqslant 0.147$
PANI Concentration (%)	$0.1 \leqslant X \leqslant 0.5$

After evaluating the experimental results and thoroughly investigating the library, the chosen range of variations was set. Adjusting these variations within the chosen ranges allows for achieving reasonable and acceptable results. Design Expert 10 software (Stat-Ease, Inc. Minneapolis, USA.) was subsequently used to fit and optimize the research, laboratory, and practical experiments. The test design table was created using the response surface methodology with a central composite design, encompassing 2 central points and 14 noncentral points.

2.6 Tests

Various tests were employed to characterize, measure, and assess the effectiveness of both the PANI nanofibers and the absorbent SH skimmers.

2.6.1 Specifications evaluation

To confirm the formation of PANI and SHCs, Fourier transform infrared spectroscopy (FTIR) (S8400, Shimadzu Company, Japan) was performed. SEM analysis was conducted via TESCAN VEGA/XMU to examine the features of synthesized PANI and various types of produced skimmers. The structure of the synthesized PANI was assessed through porosity and SS measurements, including SS area, pore volume, and pore size. These parameters were analyzed using high-accuracy gas and vapor adsorption instruments. The process involved measuring the nitrogen volume absorbed and released by the material at a steady liquid nitrogen temperature (−196 °C).

2.6.2 CA test

The CA test was used to evaluate sample superhydrophobicity. The CA was measured using the sessile drop method with a goniometer connected to a computer. A 5 μL water droplet was placed on the surface at room temperature to take the measurements. The rate of DR of the prepared coatings was measured via a rotary rheometer. In the rotating rheometer, water occupied the space between the sample coating bed and the rotating plate. The upper plate was positioned 0.2 mm from the lower plate (H = 0.2 mm). The rheometer measured the friction torque of various coatings at rotational speeds ranging from 0 to 1 000 r/min. Additionally, the produced samples underwent crude OA and DR tests according to the specifics outlined in the governing equations section.

2.6.3 OA test

A mixture of water and oil was employed to measure OA in SHCs. In a 250 ml container, a blend of 100 ml of water and 50 ml of light crude oil was combined and homogenized using a magnetic stirrer for an hour. Small SHC samples, each measuring 1 cm × 1 cm × 1 cm, were immersed in this solution for an hour. During this time, the samples absorbed both water and oil. The absorbed water weight was evaluated according to the ASTM D4006

standard. Using this data, the weight of the oil absorbed by the skimmer was determined.

3 Results and discussions

To enhance the OA and DR of the synthesized PANI, four issues have been investigated: 1) nanofiber morphology, 2) high porosity, 3) lower polarity of functional groups on the PANI chain (to accommodate more hydrocarbon chains), and 4) high CA.

3.1 Synthesized PANI

3.1.1 Chemical specification

FTIR was used to assess the chemical properties and accuracy of the synthesized polyaniline. The results were drawn via IRsolution 1.1 software, and peak analysis was performed via Origin Pro 2018. The results revealed that the spectrum of the synthesized polyaniline closely resembled that of the source PANI (Turan et al., 2021). The spectra, displayed in Figures 3–6, feature characteristic absorption bands associated with the quinoid and benzene cycles, which reflect the backbone structure across different dopants. Each dopant caused slight shifts in the position of these bands, reflecting its unique influence on the electronic environment and protonation state of the polymer. The annotated spectra clearly demonstrate these shifts, offering a comprehensive comparison of how each dopant modifies the molecular structure of PANI. These differences confirm the structural versatility of PANI, tailored by dopant-specific interactions, which could potentially influence its performance in OA and DR applications.

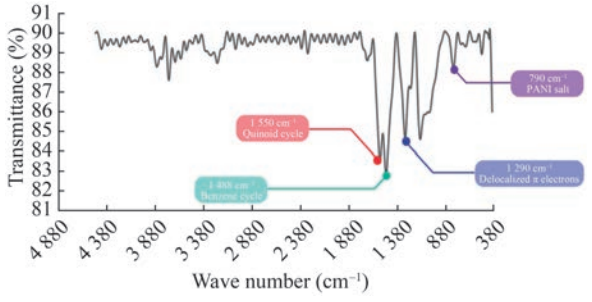

Figure 3 FTIR spectrum of PANI–MSA

3.1.2 Physical specification

To investigate the physical properties and structural morphology of the synthesized PANI with different dopants, SEM images of the samples were captured, as shown in Figure 7. Before imaging, the samples were coated with a layer of gold, as shown in Figure 7 (a) and (b). SEM images of PANI-MSA reveal that the morphology of PANI synthesized with the dopant MSA was more regular and uniform

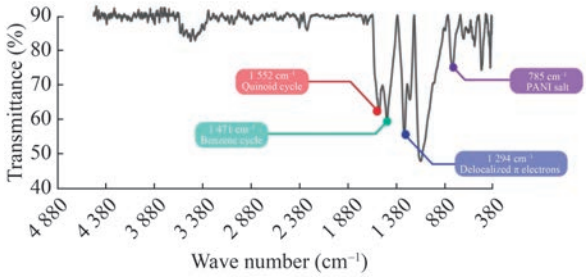

Figure 4 FTIR spectrum of PANI–HCA

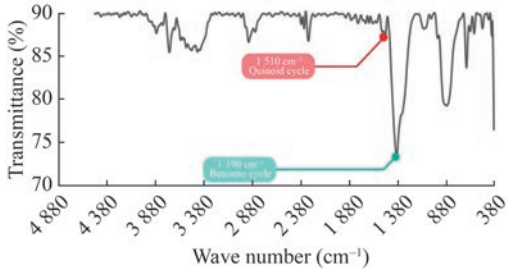

Figure 5 FTIR spectrum of PANI–SA

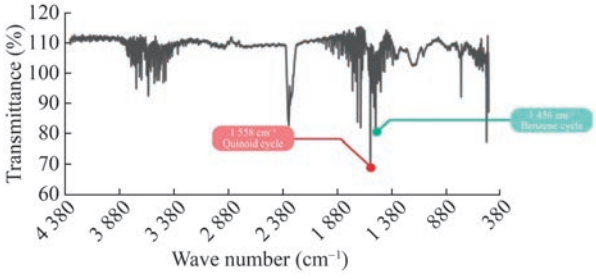

Figure 6 FTIR spectrum of PANI–NA

than that of the other dopants, forming well-defined nanofibers with a fibrous structure. These nanofibers had a particle size of 60 nm, attributed to the low permeability of the 3 000 Da membrane. The MSA-based PANI nanofibers exhibited entanglement and crowding of the formed fibers. Further results from porosity and SS area measurements, discussed in the next section, confirm that polyaniline–MSA had the smallest SS area among all tested materials. As shown in Figure 7 (c) and (d), the morphology of PANI–NA was highly porous and irregular. The approximate diameter of the formed nanofibers was 90 nm. PANI–NA had a smaller pore size compared to PANI–MSA As shown in Figure 7 (e) and (f), the morphology of PANI–sulfonic acid was porous and irregular, similar to that of polyaniline–NA. This sample had a shorter fiber length and larger hole diameter compared to other samples. The fiber diameter was approximately 100 nm. As Figure 7 (g) and (h) shows, the PANI–HCA morphology was highly porous and irregular, yet more porous than that of PANI–MSA. It had a higher porosity percentage than PANI–MSA and PANI–NA but featured smaller pore diameters compared to those of

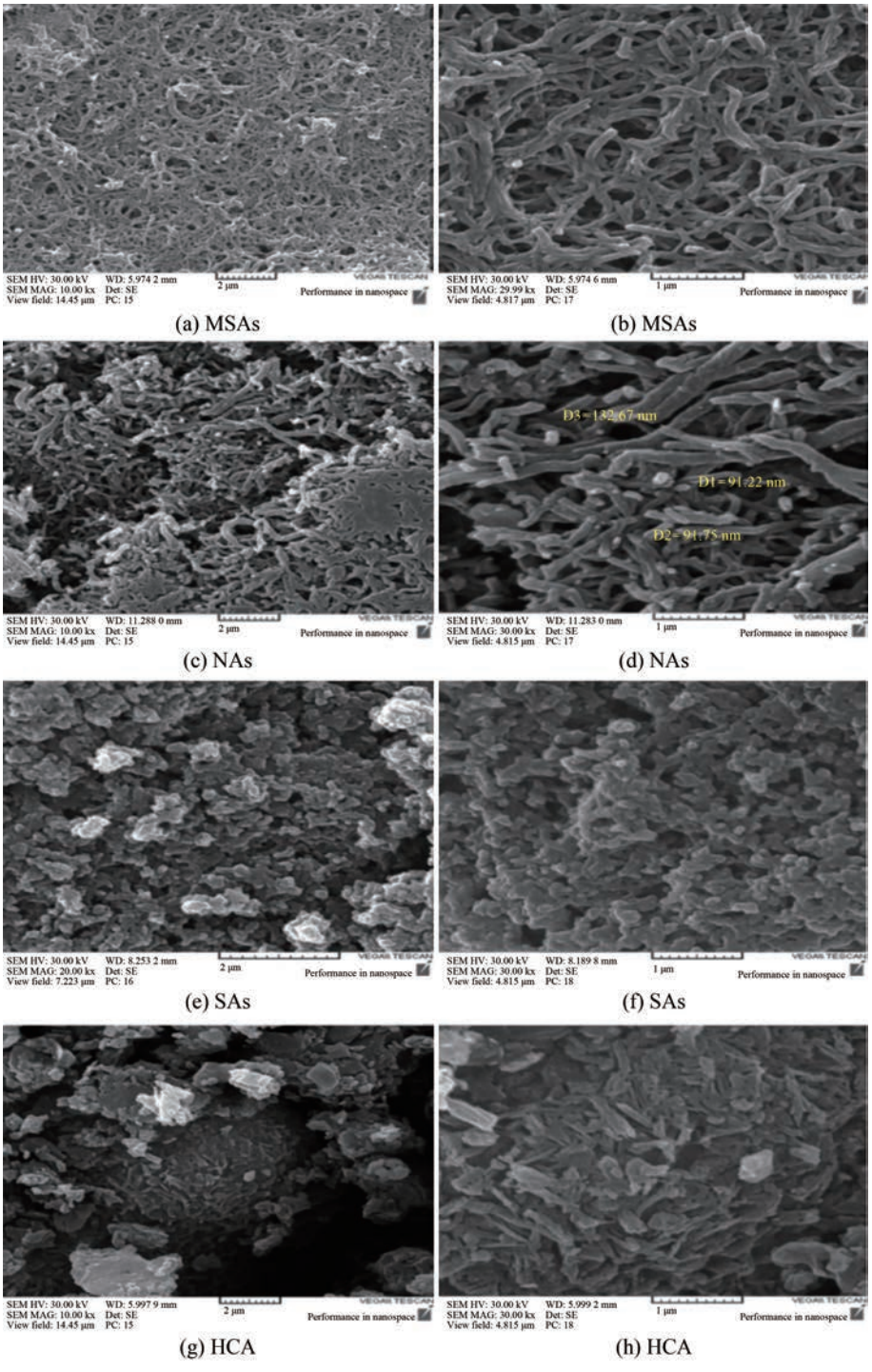

Figure 7 SEM images of PANI synthesized with dopant

the other dopants. Reducing the pore diameter and size increases the specific surface area. According to this theory, PANI–HCA is expected to exhibit the highest specific surface area among other samples. This theory is confirmed in the next section.

The differences in the morphology observed in PANI samples synthesized with various dopants can be attributed to the unique molecular interactions each dopant introduces during the polymerization process. These interactions affect the fiber formation, porosity, and overall structural characteristics. For instance, PANI–NA's smaller pore size than PANI–MSA could be attributed to the specific polymerization kinetics induced by NA, creating a denser network with narrower pores. By contrast, PANI–SA displays larger pore diameters and shorter fibers. This may be attributed to SA's influence on the polymer growth environment, pro-

moting a more open structure. PANI–HCA stands out with its highly porous and compact structure, benefiting from the molecular interactions provided by HCA, which contribute to a maximized specific surface area and enhanced porosity. These morphological variations directly impact each sample's OA and DR capabilities, as discussed further in the subsequent sections.

3.1.3 Porosity and specific surface area of PANI

The structural attributes of the synthesized PANI, such as the specific surface area, pore volume, and dimensions, were analyzed using porosity and specific surface area assessments. Figure 8 presents the adsorption and desorption isotherms of PANI samples synthesized with different dopants. The absorption isotherm of PANI–MSA shows that at a low relative pressure of up to approximately 0.8, the absorption isotherm shows a steady increase, with a gradual slope. However, beyond a relative pressure of approximately 0.9, the slope becomes steeper, indicating a rapid increase in adsorption. As shown in Figure 8, the absorption isotherms of PANI–HCA, PANI–SA, and PANI–NA follow a similar pattern. In all three graphs, up to a relative pressure of approximately 0.4, the curve indicates a consistent increase in absorption. Between relative pressures of 0.4–0.9, the slope flattens, resulting in almost constant graphs, through absorption continues to rise substantially. A comparison of the isotherm patterns of the doped PANI samples revealed that PANI–MSA has a different absorption isotherm than that of other samples of the fibrous structure of the MSA-based PANI nanofibers, as observed via SEM in Section 3.1.2.

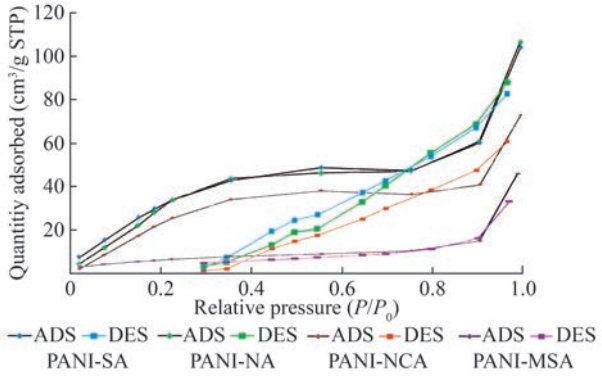

Figure 8 PANI dopant absorption and desorption isotherms

Table 4 displays the structural characteristics of the synthesized PANI samples, including the specific surface area, pore size (*d* spacing), and total pore volume (V_p). Notably, the MSA-based PANI nanofiber has the lowest specific surface area among the samples. These nanofibers exhibit smaller pore volumes compared to those of other variants, though their average pore diameters are larger. This leads to a reduced OA percentage. PANI synthesized with sulfonic acid and HCA dopants shows the highest specific surface area, indicating the highly porous nature of these samples. However, the relationship between high specific surface area and the efficiency of hydrocarbon absorption is not entirely straightforward. This is because the porosity and specific surface area analyses are based on nitrogen adsorption/desorption, whereas hydrocarbon chains are larger than nitrogen molecules. Hydrocarbon chains may not be able to access the pores that nitrogen gas can access. For this reason, relying solely on the SS area might be insufficient, and assessing the surface porosity volume of the particles is necessary. Similarly to the SS area findings, PANI doped with HCA and sulfonic acid has the largest pore volume, indicating a potentially higher sorption capacity than that of other samples. Additionally, this table shows that PANI with the HCA dopant has a smaller average hole diameter than the SA-doped variant. As a result, the holes of this sample have smaller dimensions than those of the SA-doped PANI.

Table 4 Results of porosity and SS analysis

Sample	V_p (cm³/g)	*d* spacing (nm)	SS area (m²/g)
PANI with dopant MSA	0.207 3	4.214	192.01
PANI with dopant HCA	0.383 6	3.593 6	425.16
PANI with dopant SA	0.425 6	4.525 8	741.82
PANI with dopant NA	0.284 6	3.749 7	315.46

3.2 Pure SH Film & PANI-SHC specification

3.2.1 Chemical specification

To investigate the chemical properties of the pure SHC and SHCs coatings doped with PANI, FTIR analysis was performed. Figure 9 presents the FTIR spectrum of a pure SHC, confirming the precision of the polymerization process through peak alignment with reference spectra. Figure 10 displays the spectra of the two-component SHC samples, incorporating PANI nanofibers with different dopants. The four vibrational bands observed at 1 234, 1 714, 1 595, and 2 889 cm^{-1} represent the absorption features of the SHC, while additional bands at 790, 1 470, 1 560, and 2 850 cm^{-1} provide clear evidence of PANI integration within the SHC matrix. Despite its low concentration, the bands were influenced by characteristic peaks (Tamsilian et al. 2021).

The spectra reveal distinct absorption peaks corresponding to the quinoid and benzenoid structures of PANI. Shifts in transmittance are noticeable, indicating interactions with the SHC coating matrix. These shifts, particularly around key functional groups, suggest hydrogen bonding and potential electron–donor interactions that enhance the compatibility and functionality of PANI within the SHC coating structure. The dopants significantly influence molecular interactions by modifying the electronic and structural

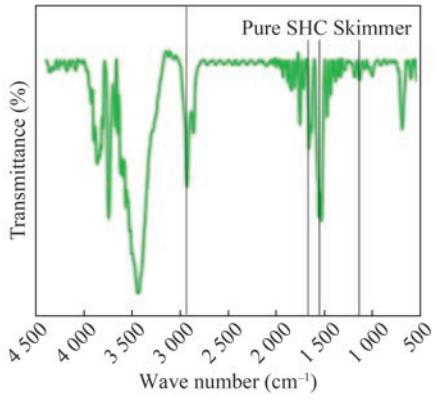

Figure 9 FTIR spectrum of a pure SHC coating

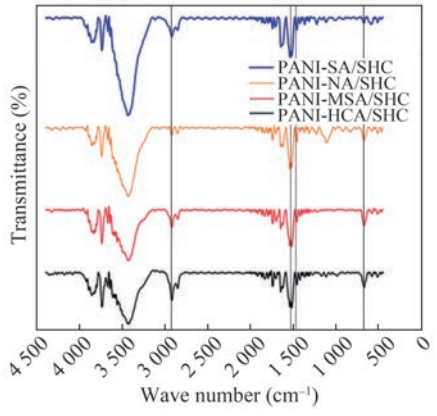

Figure 10 FTIR spectrum of SHC containing dopant PANI nanofibers

properties of PANI, leading to a more stable and integrated composite. The enhanced bonding between PANI nanofibers and the SHC coating matrix not only optimizes the skimmer performance but also improves hydrophobicity, OA, and durability. These findings highlight the crucial role of dopant selection in shaping molecular architecture and reinforce the advantage of using doped PANI in SHC coatings for advanced oil spill recovery applications.

The FTIR analysis of SHC coating–PANI composites reveals significant interactions between PANI and the SHC coating matrix, evident through key peak shifts and the emergence of new absorption features. These findings align with prior studies. For instance, Qu et al. (2024) and Shen et al. (2024) identified peak shifts and the disappearance of certain groups as evidence of chemical bonding and crosslinking, findings that align with the peak shifts observed here. Similarly, Guo et al. (2024) and Chen et al. (2024) reported strong hydrogen bonding and condensation reactions stabilizing nanocomposites, which are corroborated by the enhanced bonding and distinct peak shifts observed in this study. The presence of reactive groups and nano-rough structures, as noted by Chen et al. (2023), improved compatibility and functionality in the SHC-coating–PANI composite. Moreover, Nie et al.'s (2024) observation of new functional groups forming through chemical reactions mirrors the modifications evident in FTIR results. These findings underscore the effectiveness of dopant incorporation in optimizing molecular interactions. This not only enhances the stability and hydrophobic properties of the material but also supports its potential as a cutting-edge solution for advanced SH applications, including efficient oil spill recovery.

3.2.2 Physical specification

SEM analysis was employed to examine the morphology of the SHC samples, with a gold coating applied before imaging. SEM images of the pure SHC revealed the spherical structural morphology of the SHCs. Figure 11 shows SEM images of SHC coatings containing PANI nanofibers with different dopants. These SEM images revealed its spherical structural morphology, along with an increase in the SS area compared to that of the pure SHC coating. The improved morphology and increased SS area resulting from the incorporation of PANI are expected to greatly enhance OA and DR. Notably, the PANI–HCA dopant produced a finer pore distribution with smaller pore diameters, which led to a higher pore density per unit area. This structure offers more active sites for oil capture and boosts DR by reducing fluid resistance across the SHC surface. Supporting this, Wu et al. (2024) noted that smaller pore sizes, even at the same porosity, can improve performance and mechanical properties. These findings confirm that embedding PANI nanofibers into the SHC matrix optimizes its physical structure for environmental applications.

3.3 CA tests

The physical and chemical properties of the pure SHC coating and PANI – SHC coating samples with different dopants were analyzed, followed by measuring their CA to assess the superhydrophobicity of the coatings, as shown in Table 5. The results indicate that the PANI-SHC coating with the HCA dopant exhibited a significantly higher CA than the pure SHC. This increased CA suggests enhanced superhydrophobicity, likely resulting from the unique micro-/nano-structured surface formed by the PANI nanofibers and the chemical interactions introduced by the HCA dopant. The porous structure and smaller pore diameters observed in the HCA-doped PANI–SHC create an uneven surface topology that traps air, reducing the contact area between water droplets and the surface. This feature enhances hydrophobicity. Additionally, the chemical properties of the HCA-doped PANI contribute to a low surface energy, further promoting water repellency. This combination of surface morphology and chemical interactions is expected to enhance DR, as further discussed in the DR test section.

Recent advancements in SH materials underscore substantial progress in achieving high CAs. For example, modified silicone surfaces (Pan et al., 2025) have gained attention for their cost-effectiveness and scalability. Guo et al.

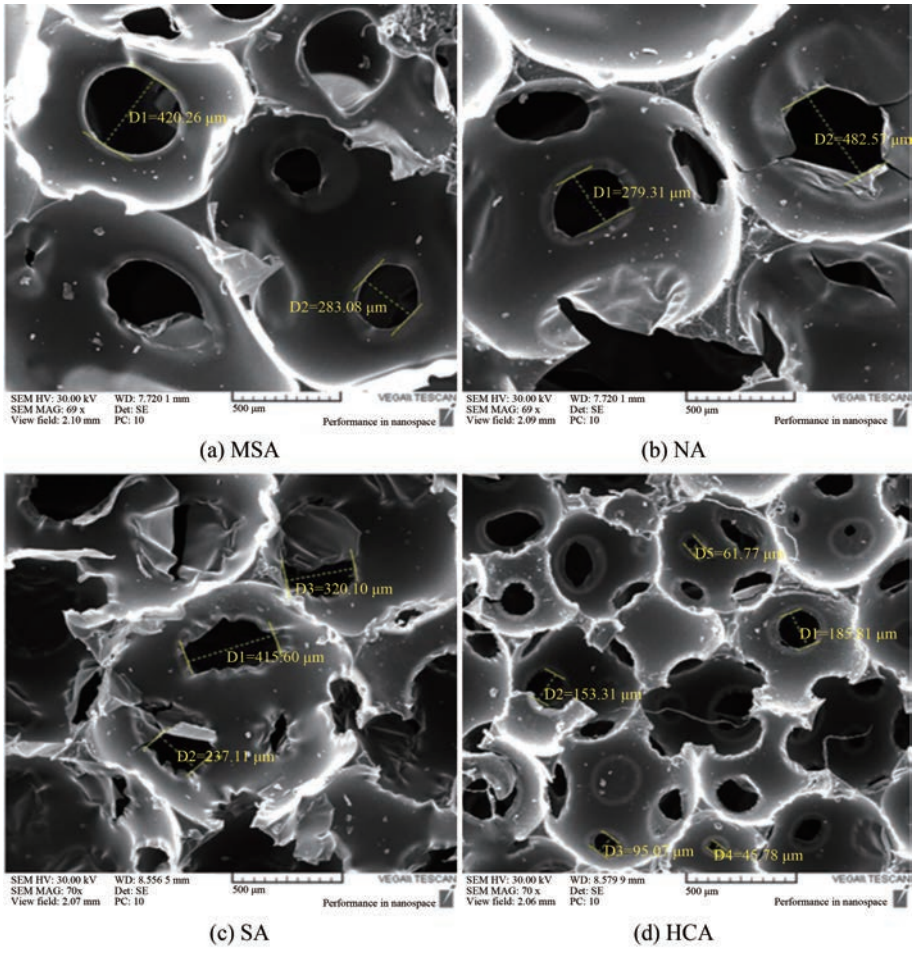

Figure 11 SEM images of SHC containing PANI with dopants

Table 5 Results of CA, DR, and OA tests

Sample	PANI synthesis method	CA (°)	DR (%)	OA (%)	Water absorption (%)	OSC
A1	Pure SHC	150	13	5.6	1.8	1.5
A2	SHC PANI synthesized with dopant MSA	153	18	7.8	1.4	2
A3	SHC containing PANI synthesized with dopant NA	159	19	8.4	1.2	3.9
A4	SHC containing PANI synthesized with dopant SA	163	23	9.6	1	4
A5	SHC containing PANI synthesized with dopant HCA	169	28	11.2	0.6	4.2

(2020) achieved a CA of 158.4° using hybrid ammonium polyphosphate/graphene oxide-coated polyurethane foam with silane functionalization. Similarly, Wu et al. (2023) reported silane-modified MXene/polybenzazole aerogels demonstrating a CA of 141°. Mao et al. (2022) designed biomimetic MXene-based networks achieving a CA of 152° owing to uniform silane molecule distribution. Zhang et al. (2021) achieved CA values exceeding 155° using microwavy nanosilica rough structures on polydimethylsiloxane foams. Furthermore, Chen et al. (2023) developed self-adhesive polydimethylsiloxane foams with MXene/CNF nanocoatings, reaching a CA of 159°. Compared to these studies, the HCA-doped PANI – SHC in this research demonstrated even higher hydrophobicity with CA measurements surpassing 169°, underscoring the superior performance and potential of this coating for advanced SH applications.

3.4 DR tests

To comprehensively assess the impact of different dopants on the DR properties of PANI-coated skimmers, a series of DR tests were conducted. These tests assess how changes in the physical and chemical structures of PANI nanofibers, influenced by specific dopants, can reduce fric-

tional resistance and enhance skimmer efficiency. Optimizing the performance of these coatings is critical in optimizing skimmer systems for effective oil spill recovery, as reduced drag directly correlates with energy efficiency and operational effectiveness. Key surface characteristics such as hydrophobicity, pore size, and surface roughness play a central role in determining DR. Modifying these properties with dopants changes how the skimmer surface interacts with water, potentially creating thinner, lower-friction boundary layers. In particular, a high CA associated with SH surfaces can facilitate air entrainment and minimize water contact, thereby decreasing drag. This section presents a comparative analysis of the DR performance across different dopant-modified PANI coatings, aiming to identify the dopant that optimally improves skimmer efficiency through enhanced hydrodynamic properties. The results provide insights into scaling PANI-coated skimmers for industrial applications that prioritize DR and energy efficiency.

Table 5 presents the DR rates of various coatings, revealing that PANI nanofiber coatings with various dopants significantly enhanced skimmer efficiency. The HCA-doped coating (A5) achieved the best results, reducing drag by 28%, compared to reductions of 23% with SA (A4) and 19% with NA (A3). These results underline the key role of the HCA dopant in improving the hydrodynamic properties of the coatings, while other dopants delivered less substantial improvements. Differences in DR performance across samples arise from variations in the microstructural and chemical characteristics of the PANI nanofibers. Dopants influence the surface CA, thereby adjusting the hydrophobicity of the coating and its interaction with water flow. The unique microstructure of the HCA-doped PANI increases the CA, resulting in a more effective DR. Reduced friction not only enhances oil spill recovery efficiency but also decreases energy consumption, making skimmers with optimized PANI-coated surfaces more energy-efficient. These findings demonstrate the potential for scaling up PANI-coated skimmer systems in industrial applications, offering both economic and environmental benefits.

3.5 Crude OA tests

To thoroughly evaluate the OA capacity and selectivity of PANI-enhanced SHC coatings, a series of crude OA tests were conducted on samples modified with different dopants. These tests are crucial for evaluating the coatings' oleophilic (oil-attracting) and hydrophobic (water-repellent) properties of each coating, both of which are essential for effective oil spill recovery applications. By measuring the amounts of oil and water each sample absorbs, this test provides insights into the role of dopant-induced changes in the microstructure, pore size, and surface chemistry of the coatings. Enhanced surface roughness and pore distribution through certain dopants may increase the coating's oil affinity while minimizing water uptake. The results presented in this section compare the crude OA performance of PANI–SHC coatings doped with MSA, NA, SA, and HCA to identify the dopant that yields the highest OA efficiency with minimal water uptake, an ideal combination for environmental remediation and resource recovery applications.

The crude OA test results (Table 5) revealed notable differences among the samples. The pure SHC absorbed 5.6 ml of oil and 1.8 ml of water. SHC coatings with PANI nanofibers doped with MSA showed absorption of 7.8 ml of oil and 1.4 ml of water. Additionally, SHC containing PANI nanofibers doped with NA absorbed 8.4 ml of oil and 1.2 ml of water. The SHC with PANI nanofibers doped with SA absorbed 9.6 ml of oil and 1 ml of water, while that containing PANI nanofibers doped with HCA absorbed 11.2 ml of oil and only 0.6 ml of water. Table 5 presents the crude OA test results, indicating that the use of HCA-doped PANI nanofibers achieved the most favorable outcomes in terms of OA and minimal water uptake, consistent with the CA and OA results.

3.6 Redoped PANI-SHC

To optimize the OA, CA, and DR properties of PANI–SHC coatings, a dedoping–redoping process was applied to the PANI structure originally doped with MSA. This process involves removing the initial MSA dopant (dedoping) and then introducing HCA as a new dopant (redoping). These changes are designed to refine the coating's porous structure, specifically by achieving smaller, more uniformly distributed pores that increase the SS area and enhance interactions with oil while repelling water. The introduction of HCA as a dopant aims to elevate the CA by increasing surface roughness and reducing surface energy, which is essential for achieving superhydrophobicity. This refined pore structure and enhanced hydrophobic properties create an air-trapping layer that significantly minimizes water interaction, reduces friction, and improves DR. This section presents a detailed comparison of the performance metrics (CA, DR, and OA) of the redoped PANI–SHC sample, highlighting its enhanced efficiency in oil spill recovery applications compared to previously tested samples.

The SH–PANI coating doped with MSA originally exhibited a fibrous nature and densely woven structure with large pores and greater diameters compared to other samples. To improve its performance, the structure was modified to achieve smaller and more uniform pores, optimizing both OA and CA. This modification involved a dedoping process for the MSA-doped PANI, followed by redoping with HCA. The dedoping was conducted using 0.1 M hydroxyl ammonium to remove the MSA dopant. This was followed by redoping with 0.5 M HCA using dialysis tubing to introduce a new HCA dopant into the PANI structure. This modification refined the PANI fibers, resulting in a smaller, optimized pore diameter to improve OA and achieve a

higher CA. After the procedure, new PANI nanofibers were obtained after washing and drying, and an SH–PANI film containing new nanofibers formed. Tests were conducted for CA and DR evaluation. The CA test revealed a measurement of 175° for this sample, indicating a higher CA than those of previous samples. The drag test exhibited a measured DR of 32%, surpassing previous results. During OA testing, the coating absorbed 6.6 ml of oil with minimal water uptake of only 0.3 ml. The OSC for this specific sample was determined to be 4.6. A comparison between this sample's results with prior results underscores the effectiveness of combining a well-structured porous composition along with reduced pore diameters among the PANI fibers. This enhanced structural composition significantly improved performance across CA, DR, and OA metrics.

3.7 Optimization of the PANI-Added coating

To maximize the performance of PANI-coated SHCs for OA and hydrophobicity, a systematic optimization was conducted using response surface methodology (RSM). This approach enabled the evaluation of key factors—such as PANI concentration, APS/aniline ratio, and acid/aniline ratio—that impact the CA, OA, and cost, essential for developing an efficient and cost-effective coating. Sixteen samples were prepared using a factorial design to examine the effects of these variables and their interactions. The optimization process involved modeling the responses (CA, OA, and cost) using regression analysis and validating the model accuracy through analysis of variance (ANOVA). RSM helped identify models that closely matched experimental data, highlighting the most influential parameters for each performance metric. This section presents the ANOVA results, including model fit values (R^2, p-values) and the optimal conditions that achieved the highest OA and CA values while minimizing costs. SEM images of the optimal sample are included to illustrate the microstructural features contributing to the enhanced performance. This optimized composition offers potential for large-scale applications, balancing oil recovery efficiency, water repellency, and cost-effectiveness. Detailed experimental methods and ANOVA results can be found in Appendix A.

The analysis highlights how the key design parameters impact the fundamental properties of the skimmer coating, specifically its hydrophobicity, oil absorption capability, and cost. Figures 12–14 present insights into the roles of PANI concentration, APS/aniline ratio, and acid/aniline ratio in influencing CA, OA, and cost. Figure 12 shows that increasing any parameter leads to a linear reduction in CA, with the highest sensitivity observed for PANI concentration. This suggests that higher PANI concentration levels reduce surface hydrophobicity by altering the coating's microstructure and surface energy. Figure 13 illustrates that the acid/aniline ratio positively affects OA,

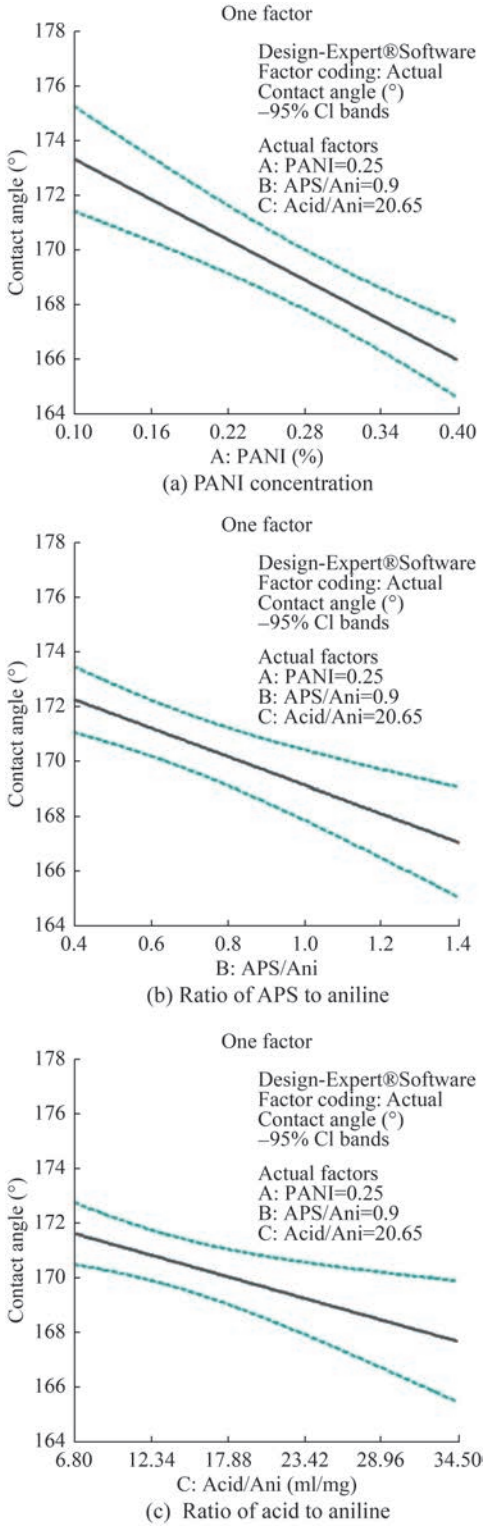

Figure 12 Impact of design parameters on CA outcomes

enhancing oil sorption capabilities, while the APS/aniline ratio has minimal influence on OA. This indicates that higher acid concentrations are critical for improving oil retention by meeting the microstructural requirements for porosity. Conversely, Figure 14 shows that the acid/aniline

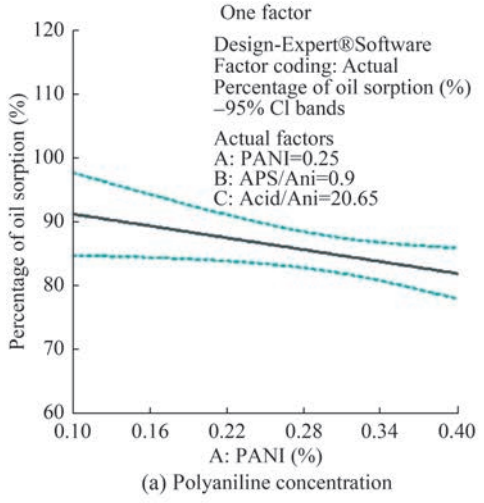

(a) Polyaniline concentration

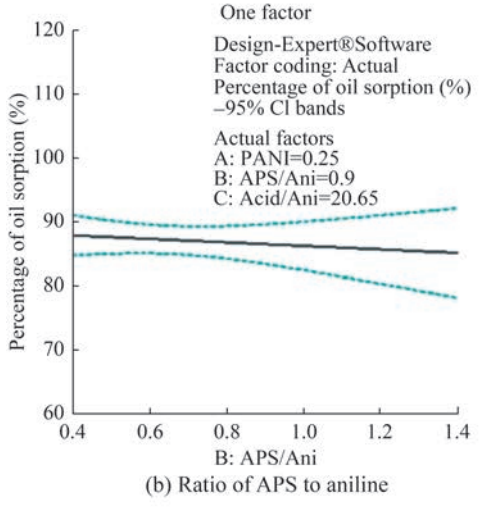

(b) Ratio of APS to aniline

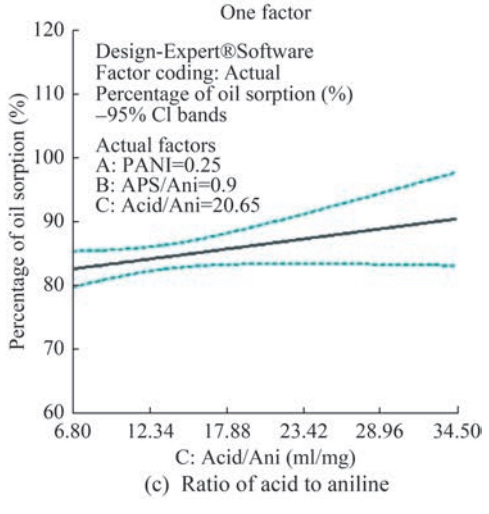

(c) Ratio of acid to aniline

Figure 13 Impact of the design parameters on the OA response

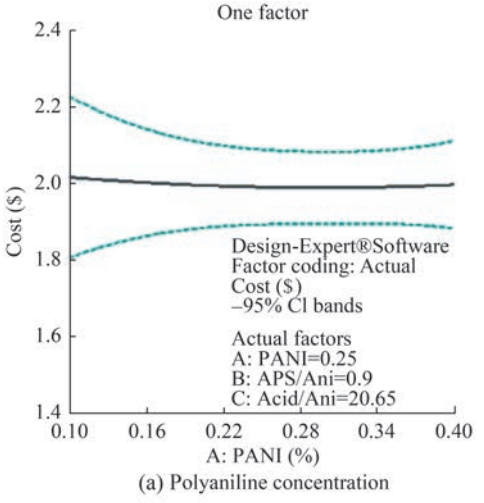

(a) Polyaniline concentration

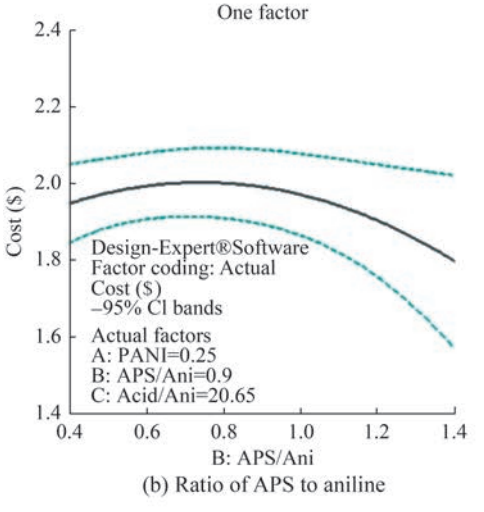

(b) Ratio of APS to aniline

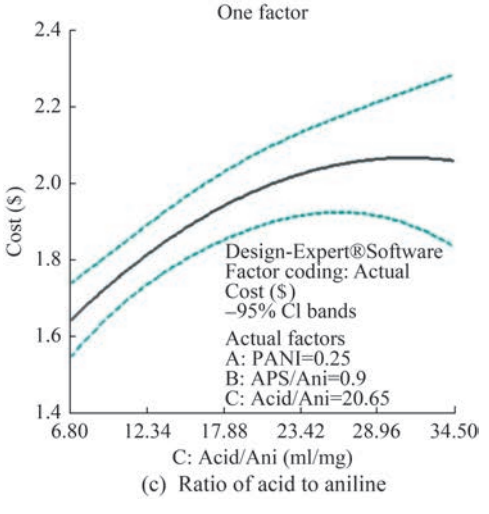

(c) Ratio of acid to aniline

Figure 14 Impact of the design parameters on the cost response

ratio significantly affects cost owing to the higher price of acid, while PANI concentration has little effect on cost. This suggests that optimizing the acid/aniline ratio is crucial for achieving superior OA and cost efficiency. By contrast, fine-tuning the PANI concentration is crucial for maintaining the desired hydrophobic properties, as it significantly influences the CA. This multi-faceted optimization enables the development of a high-performance, cost-effective skimmer coating tailored for effective oil spill management.

The results presented in Figures 15 through 17 highlight

the interactions among key design parameters and their effects on CA, OA, and cost, critical factors for optimizing the performance and economic feasibility of the coating. Figure 15 illustrates how reducing PANI concentration and increasing the APS-to-aniline ratio positively impact the CA, improving superhydrophobicity. This enhancement indicates that optimizing PANI concentration and adjusting the APS-to-aniline ratio can significantly enhance the coating's water-repellent properties, which is beneficial for reducing drag force on the skimmer. Achieving a higher CA is crucial for maximizing oil spill recovery efficiency, as it enhances the coating's ability to repel water while selectively absorbing oil. Figure 16 examines the influence of these parameters on OA. Increasing the APS-to-aniline ratio while keeping the PANI concentration constant linearly increases oil sorption. However, increasing PANI concentration causes a notable decrease in oil sorption, indicating a complex relationship between these parameters and the coating's OA efficiency. This finding suggests a trade-off between the two factors; while a higher APS-to-aniline ratio supports greater oil uptake, excessive PANI concentration can hinder the coating's absorptive capacity. Balancing these parameters is, therefore, essential for achieving maximum OA efficiency. Figure 17 explores the cost implications of these design parameters. The results indicate that production costs initially rise and then decline with increases in the APS-to-aniline or acid-to-aniline ratios. The acid-to-aniline ratio has the largest impact on cost owing to the relatively high cost of acid. This indicates that optimizing these ratios is crucial for developing a cost-effective coating. Achieving high-performance coatings with minimized production costs is vital for potential large-scale commercial applications, where economic viability is as important as performance efficiency. This comprehensive analysis underscores the importance of balancing design parameters to optimize coating performance while managing costs.

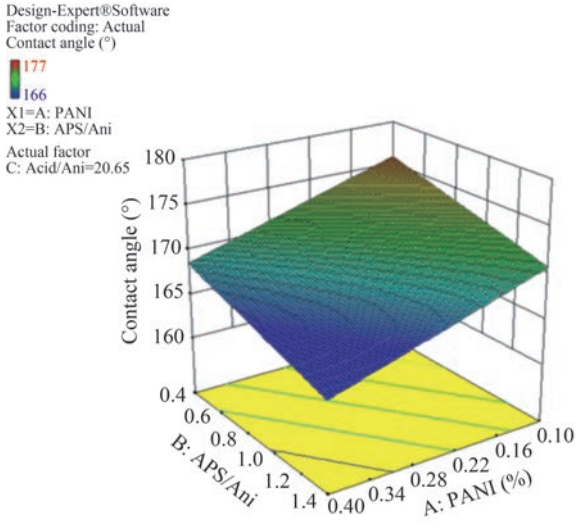

Figure 15 Effects of APS/aniline and PANI on the CA

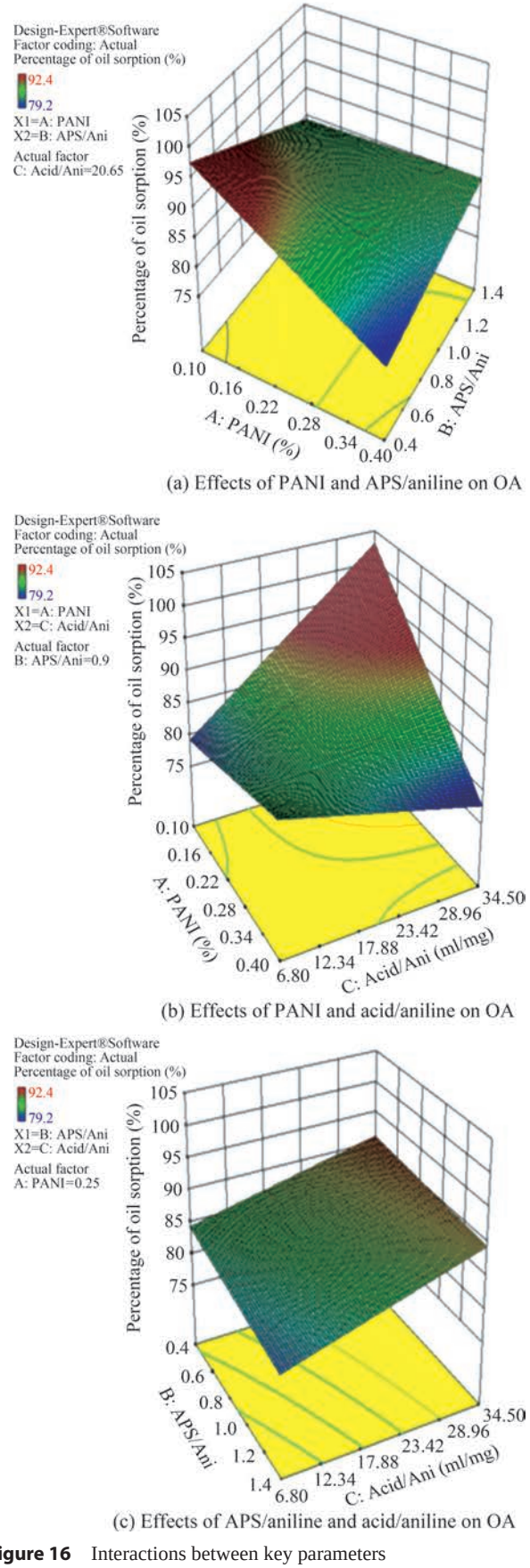

Figure 16 Interactions between key parameters

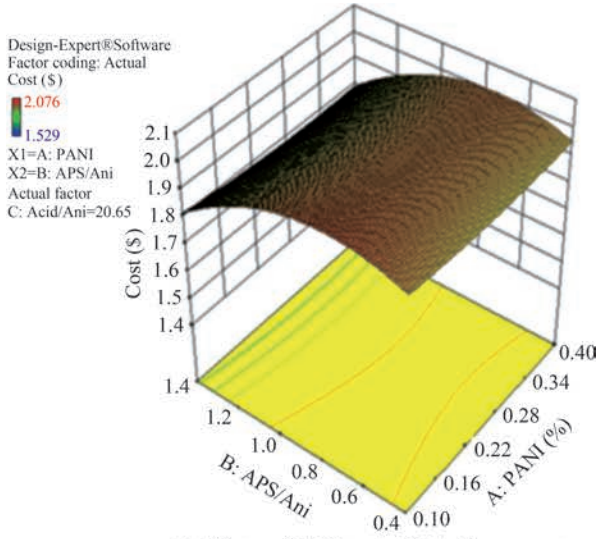

(a) Effects of PANI and APS/aniline on cost

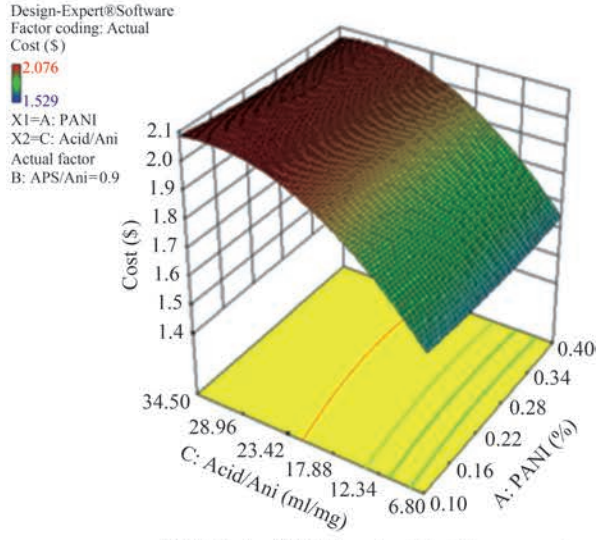

(b) Effects of PANI and acid/aniline on cost

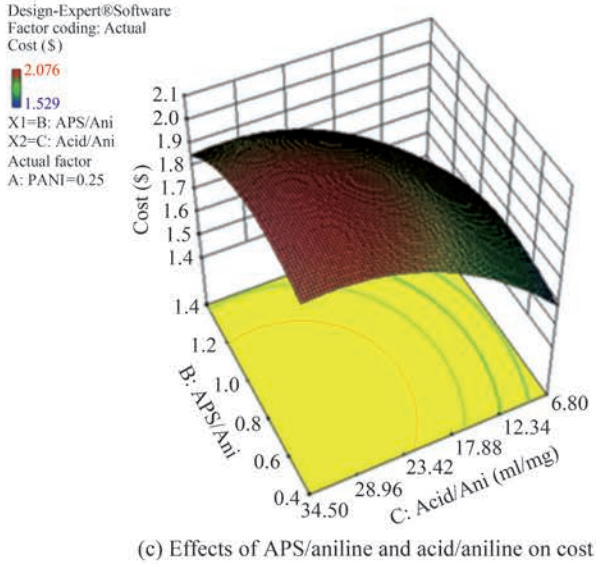

(c) Effects of APS/aniline and acid/aniline on cost

Figure 17 Interactions between key parameters

Table 6 presents the optimal values using response surface methodology. The best-performing coating containing PANI nanofibers achieved a CA of 177.477°, an OA efficiency of 88.725%, a production cost of $1.710, and a desirability rate of 78.5%. A test was conducted to validate and confirm the optimization based on the values outlined in Table 6. Figure 18 presents SEM images of the optimal coating sample incorporating PANI nanofibers. As shown in Figure 18, the coating's high CA, and consequently its enhanced DR and OA, can be attributed to its morphology, which features a regular spherical structure and an acceptable SS area.

3.8 Comparison with other novel methods

Efforts to develop advanced oil spill recovery methods have grown significantly in recent years, focusing on innovative solutions that leverage advanced technologies. One promising method involves the use of carbon nanofiber foams produced by electrospinning. These foams feature an exceptionally high surface area of nanofibers, enabling rapid and effective OA. Studies have demonstrated that these materials can absorb more than 20 times their weight in oil. However, despite their impressive performance, this approach faces challenges. High production costs and complex manufacturing processes make these foams less practical for widespread use. Additionally, their mechanical properties often limit their reusability, further limiting their potential for large-scale industrial applications.

Another popular technique utilizes SH polymeric materials, such as polyurethane, which is modified to repel water while effectively absorbing oil. This method enhances the polyurethane surface with SHCs, allowing it to selectively absorb oil while repelling water. However, these materials lose efficiency in harsh environmental conditions, such as areas with strong waves or large contaminants. Moreover, owing to the intrinsic limitations of polymer-based materials, their durability is often compromised, leading to shorter lifespans and a need for frequent replacement.

By contrast, the method proposed in this study, employing PANI nanofibers, offers several key advantages over these methods. The structure of PANI nanofibers, with their high surface area and hydrophobic properties, greatly boosts OA efficiency. Unlike carbon-based materials, which are expensive to produce, PANI nanofibers are derived from more affordable materials, simplifying their fabrication process. Moreover, PANI coatings exhibit superior mechanical properties and excellent resistance to harsh environmental conditions, resulting in a longer operational life than SH polymeric materials.

A standout feature of this approach is its DR capability, which leads to lower energy consumption. The SHCs created with PANI improve OA and reduce drag on skimmer surfaces, cutting fuel consumption. This addresses a critical

Table 6 Optimal values derived from response surface methodology

Sample	A: PANI (%)	B: APS/ Aniline	C: Acid/Aniline (ml/mg)	R1: CA (°)	R2: Percentage of OA	R3: Cost ($)	Desirability (%)
Optimal sample	0.1	0.4	9.689	177.477	88.725	1.710	78.5

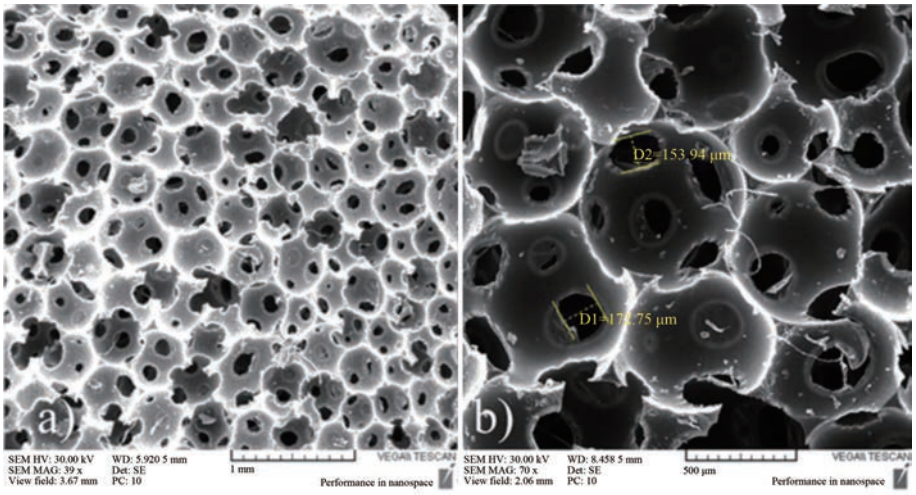

Figure 18 SEM images of the optimal nanofiber coating

gap in many other modern techniques, which often overlook energy efficiency during the oil collection process. Consequently, by combining high absorption capacity, lower production costs, and energy efficiency, the proposed method presents a competitive and sustainable alternative to existing oil spill collection technologies.

4 Conclusions

This study focused on optimizing a novel oil spill removal skimmer using SH–PANI nanofiber coatings. The key goals were to maximize OA, CA, and DR while minimizing production costs. Among the dopants used, HCA-doped PANI demonstrated the highest porosity, smallest pore diameter, and superior SH properties, contributing significantly to OA and DR performance. To enhance the fibrous structure and hydrophilic properties, an adjustment was made to the doping process. Initially, MSA was used to dope the PANI nanofibers, but it was later removed in a dedoping step and replaced with HCA in a redoping process. This change led to smaller pore sizes, increased hydrophobicity, and improved OA. Following these modifications, the optimized coating achieved a CA of 177.5°, an OA of 88.7%, a DR rate of 32%, and a cost of $1.71. These results highlight the skimmer's potential as a cost-effective, efficient solution for oil spill cleanup, aligning with global environmental goals to reduce energy consumption and emissions.

Nomenclature

PANI	Polyaniline
PU	Polyurethane
NA	Nitric acid
SA	Sulfuric acid
MSA	Methanesulfonic acid
APS	Ammonium per sulfate
SEM	Scanning electron microscope
SS	Specific surface
SH	Super hydrophobic
HCA	Hydrochloric acid
DR	Drag reduction
CA	Contact angle
OA	Oil absorption
OSC	Oil sorption coefficient
FTIR	Fourier transform infrared spectroscopy
M	Molar
SHC	Super hydrophobic coat

Appendix A

This appendix details the experimental design and optimization process aimed at maximizing OA and CA while minimizing cost. 16 SHC samples with MSA-based PANI nanofibers were prepared and optimized through a dedoping-

redoping process with HCA. Tables A1 to A6 present the key findings from RSM and an ANOVA, highlighting the most impactful design parameters.

In this section, the objective is to find the optimal values of the effective parameters to reach the highest percentage of OA and CA with the lowest cost. After the experimental design values were determined, 16 samples of MSA-based PANI nanofibers were first dedoped and then redoped with HCA. Sixteen samples of SHC containing PANI nanofibers were subsequently prepared. To comprehensively assess and examine the efficacy of the produced coatings, all 16 samples were tested for OA and CA. Table A1 lists the operational expenses, OAs, and CAs associated with the 16 samples.

Once the test design table is finalized, leveraging response surface methodology tools enables the attainment of the most favorable outcome by considering independent input parameters. This methodology's primary goal involves implementing and adjusting the regression model to align with the outcomes derived from the conducted test. Consequently, for scrutinizing practical outcomes, the utilization of analysis of variance (ANOVA) becomes crucial, serving as a pivotal tool to validate the regression model's adherence to each response. The outcomes of this analysis are presented in Table A2.

Table A1 Test design

No.	Factor 1	Factor 2	Factor 3	Response 1	Response 2	Response 3
	A: PANI	B: APS/Aniline	C: Acid/Aniline	CA	Percentage of OA	Cost
	%	ml/mg	ml/mg	°	%	$
1	0.1	0.6	11.4	176	88.8	1.802
2	0.2	0.4	20.4	174	92.4	1.927
3	0.2	0.4	7.9	177	84	1.653
4	0.2	1	20.4	170	87.6	1.967
5	0.2	1	7.9	173	81.6	1.695
6	0.3	1.4	11.4	168	82.8	1.585
7	0.3	0.6	11.4	169	85.2	1.802
8	0.3	0.6	6.8	171	83.4	1.529
9	0.3	0.6	11.4	169.5	87.6	1.802
10	0.3	0.4	11.4	173	81.6	1.786
11	0.3	0.6	34.5	168	84	2.076
12	0.3	0.6	11.4	170	80.4	1.802
13	0.4	1	7.9	167	86.4	1.695
14	0.4	0.4	7.9	172	82.8	1.653
15	0.4	0.4	20.4	169	79.2	1.927
16	0.4	1	20.4	166	84	1.967

Table A2 ANOVA outcomes related to the created models

Response	Model	R^2	Adj-R^2	Pre-R^2	p value	Selection
R1: CA (°)	Linear	0.869 9	0.837 4	0.803 7	<0.000 1	Selected
	2FI	0.872 6	0.787 7	0.675 0	0.977 7	
	Quadratic	0.948 7	0.871 7	−0.925 7	0.119 5	
R2: Percentage of OA (%)	Linear	0.26	0.075	−0.307 6	0.289 1	
	2FI	0.723 9	0.539 9	0.171 8	0.025 5	Selected
	Quadratic	0.811 4	0.528 5	0.206	0.482 8	
R3: Cost ($)	Linear	0.798 8	0.748 5	0.519 4	0.000 2	
	2FI	0.812 5	0.687 5	0.187 4	0.881	
	Quadratic	0.946 9	0.867 3	0.165 2	0.044	Selected

The main elements within ANOVA, such as R^2, which represents the model's correlation coefficient (tends to 1), and the p value, which indicates the model's significance (p value < 0.05), were employed in choosing the most suitable model. According to the components, the linear model (p value ⩽ 0.000 1, R^2 = 0.869 9) was used for the CA response, the 2FI model (p value = 0.025 5, R^2 = 0.723 9) was used for the percentage of OA response, and the quadratic model (p value = 0.044, R^2 = 0.946 9) was selected for the cost response. Tables A3, A4, and A5 show the results of the ANOVA for the CA response (R1), percentage of OA response (R2), and cost response (R3).

The p value of the model, as illustrated in Table A4 is significantly less than 0.05, indicating strong alignment between the model and the experimental outcomes of the CA test. Moreover, the lack of fit p value, associated with the pure error and indicative of the model's repeatability and error measure, surpassed 0.05 (p value=0.122 1), indicating that the selected model fully matches the input data. The higher F values for each parameter indicate the more significant effect that the parameter has on the model. Hence, the PANI concentration has the most significant effect on the CA, followed by the molarity ratio of APS to aniline and the molarity ratio of acid to aniline.

On the basis of the outcomes presented in Table A5, the model's p value falling below 0.05 suggests a complete alignment between the model and the practical data acquired from the OA test. Additionally, the lack of fit values associated with the pure error, which exceeds 0.05, further signifies the complete correspondence between the model and the practical outcomes. The F values for the parameters indicate that the PANI concentration parameter, followed by the M ratio of acid to aniline, has the most substantial influence on the percentage of OA.

Table A3 Results of ANOVA for the CA response (R1)

Source	Sum of squares	df	Mean square	F value	p value	Selection
Model	130.04	3	43.35	26.75	< 0.000 1	Significant
A-PANI	70.29	1	70.29	43.38	< 0.000 1	
B-APS/Aniline	36.54	1	36.54	22.55	0.000 5	
C-Acid/Aniline	16.66	1	16.66	10.28	0.007 5	
Residual	19.44	12	1.62			
Lack of Fit	18.94	10	1.89	7.58	0.122 1	Not significant
Pure Error	0.50	2	0.25			
Cor Total	149.48	15				

Table A4 Results of ANOVA for the percentage of OA response (R2)

Source	Sum of squares	df	Mean square	F value	p value	Selection
Model	125.73	6	20.95	3.93	0.032 8	Significant
A-PANI	31.11	1	31.11	5.84	0.038 8	
B-APS/Aniline	2.59	1	2.59	0.49	0.503 3	
C-Acid/Aniline	20.16	1	20.16	3.78	0.083 6	
AB	35.37	1	35.37	6.64	0.029 9	
AC	48.54	1	48.54	9.11	0.014 5	
BC	0.18	1	0.18	0.034	0.858 4	
Residual	47.95	9	5.33			
Lack of Fit	21.07	7	3.01	0.22	0.943 8	not significant
Pure Error	26.88	2	13.44			
Cor Total	173.68	15				

As depicted in Table A5, the model's p value is significantly below 0.05, suggesting a solid alignment between the model and the practical results. The highest F value is related to the molarity ratio of acid to aniline, indicating that it has the most significant effect on the cost. A pure error value of zero and an undefined F value for LOF indicate the absence of errors in repetitions. Upon creating a model that exhibits an excellent fit for the responses of CA (R1), percentage of OA (R2), and cost (R3), a polynomial equation incorporating the influential design parameters and their interactions was derived (Table A6).

Based on the experimental design and ANOVA analysis, the optimization results were further validated by comparing the model's predictions with actual experimental data. Figure A1 shows the alignment between the model's predicted results and the experimental outcomes. Upon comparing the experimentally obtained results with the predicted outcomes derived from the model, considering the coefficients for each response, it becomes evident that the developed model effectively aligns with the experimental results for CA, OA, and cost.

Table A5 Results of ANOVA for the cost response (R3)

Source	Sum of squares	df	Mean square	F value	p value	Selection
Model	0.33	9	0.037	11.90	0.003 5	Significant
A-PANI	1.068×10^{-4}	1	1.068×10^{-4}	0.035	0.858 4	
B-APS/Aniline	6.003×10^{-3}	1	6.003×10^{-3}	1.95	0.212 2	
C-Acid/Aniline	0.045	1	0.045	14.65	0.008 7	
AB	3.936×10^{-6}	1	3.936×10^{-6}	1.278×10^{-3}	0.972 6	
AC	6.914×10^{-6}	1	6.914×10^{-6}	2.245×10^{-3}	0.963 7	
BC	4.985×10^{-5}	1	4.985×10^{-5}	0.016	0.902 9	
A^2	4.981×10^{-4}	1	4.981×10^{-4}	0.16	0.701 5	
B^2	0.023	1	0.023	7.52	0.033 6	
C^2	0.028	1	0.028	9.22	0.022 9	
Residual	0.018	6	3.080×10^{-3}			
Lack of Fit	0.018	4	4.620×10^{-3}			
Pure Error	0.000	2	0.000			
Cor Total	0.35	15				

Table A6 Calculated coefficients corresponding to each response term

Factor	R1: CA		R2: Percentage of OA		R3: Cost	
	Coefficient EST	Standard error	Coefficient EST	Standard error	Coefficient EST	Standard error
Constant	+183.387 05	0.53	+88.026 19	1.38	+1.147 85	0.040
A-PANI	−24.516 59	0.56	−14.138 65	1.93	−0.366 66	0.052
B-APS/Aniline	−5.197 83	0.55	−21.509 07	1.96	+0.736 94	0.055
C-Acid/Aniline	−0.142 40	0.62	+1.174 64	2.02	+0.046 177	0.054
AB			+68.953 73	2.01	−0.023 254	0.049
AC			−3.829 49	2.64	$-1.473\ 38\times10^{-3}$	0.065
BC			+0.074 158	2.80	$-1.311\ 38\times10^{-3}$	0.071
A^2					+0.707 86	0.040
B^2					−0.475 77	0.043
C^2					$-7.167\ 91\times10^{-4}$	0.045

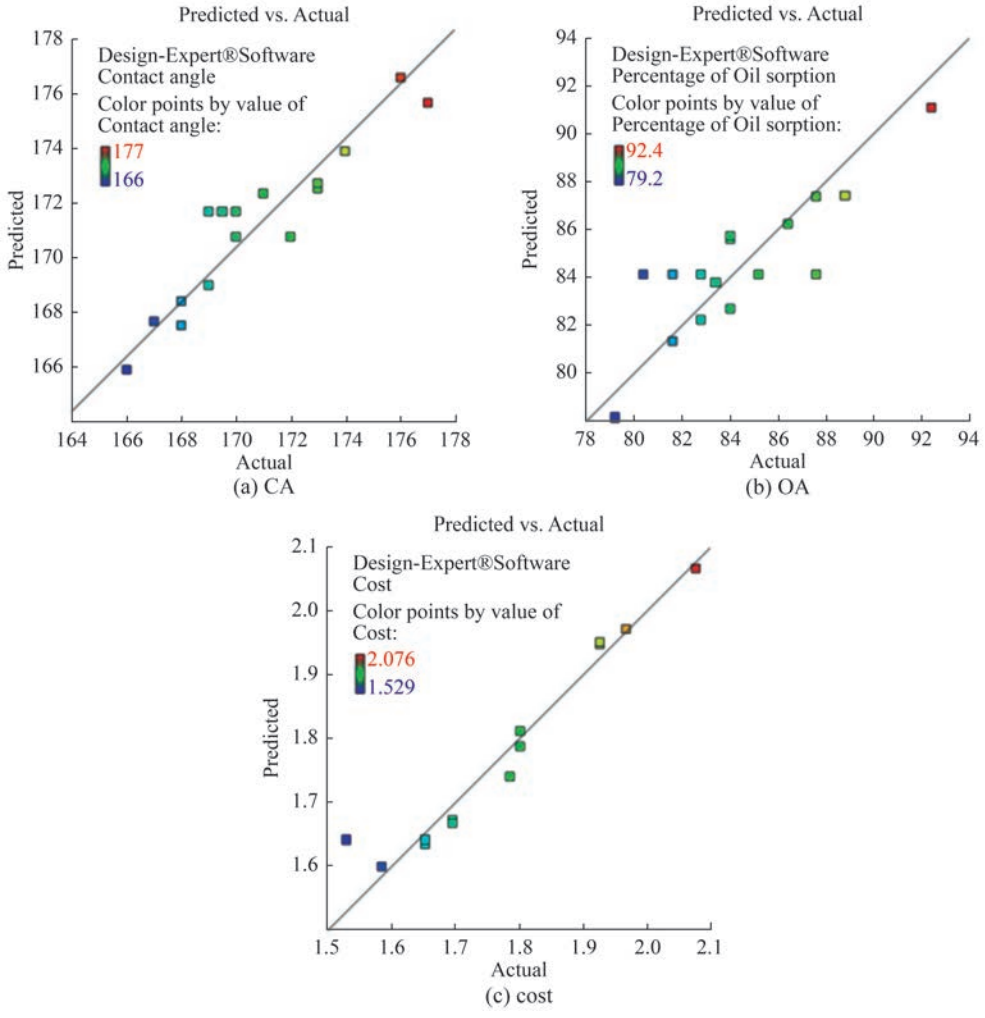

Figure A1 Model's predicted results and actual experimental outcomes for the following responses

Competing interest The authors have no competing interests to declare that are relevant to the content of this article.

References

Abidli A, Huang Y, Cherukupally P, Bilton AM, Park CB (2020) Novel separator skimmer for oil spill cleanup and oily wastewater treatment: From conceptual system design to the first pilot-scale prototype development. Environmental Technology & Innovation 18: 100598. https://doi.org/10.1016/j.eti.2019.100598

Baig U, Faizan M, Sajid M (2021) Effective removal of hazardous pollutants from water and deactivation of water-borne pathogens using multifunctional synthetic adsorbent materials: A review. Journal of Cleaner Production 302: 126735. https://doi.org/10.1016/j.jclepro.2021.126735

Bhaumik M, McCrindle RI, Maity A, Agarwal S, Gupta VK (2016) Polyaniline nanofibers as highly effective re-usable adsorbent for removal of reactive black 5 from aqueous solutions. Journal of Colloid and Interface Science 466: 442-451. https://doi.org/10.1016/j.jcis.2015.12.056

Chen HY, Chen ZY, Mao M, Wu YY, Yang F, Gong LX, Zhao L, Cao CF, Song P, Gao JF, Zhang GD, Shi YQ, Cao K, Tang LC (2023) Self-adhesive polydimethylsiloxane foam materials decorated with mXene/cellulose nanofiber interconnected network for versatile functionalities. Advanced Functional Materials 33(48): 2304927. https://doi.org/10.1002/adfm.202304927

Chen HY, Li Y, Wang PH, Qu ZH, Qin YQ, Yang L, Li JY, Gong LX, Zhao L, Zhang GD, Gao JF, Tang LC (2024) Facile fabrication of low-content surface-assembled MXene in silicone rubber foam materials with lightweight, wide-temperature mechanical flexibility, improved flame resistance and exceptional smoke suppression. Composites Part A: Applied Science and Manufacturing 177: 107907. https://doi.org/10.1016/j.compositesa.2023.107907

Chuah LF, Mohd Amin M, Yusup S, Raman NA, Bokhari A, Klemeš JJ, Alnarabiji MS (2016) Influence of green catalyst on transesterification process using ultrasonic-assisted. Journal of Cleaner Production 136: 14-22. https://doi.org/10.1016/j.jclepro.2016.05.003

Feng YY, Hu H, Peng GY, Zhou Y (2020) Microbubble effect on friction drag reduction in a turbulent boundary layer. Ocean Engineering 211: 107583. https://doi.org/10.1016/j.oceaneng.2020.107583

Ghorbankhani A, Zahedi AR (2022) Micro-cellular polymer foam supported polyaniline-nanofiber: Eco-friendly tool for petroleum oil spill cleanup. Journal of Cleaner Production 368: 133240. https://doi.org/10.1016/j.jclepro.2022.133240

Gose JW, Golovin K, Boban M, Tobelmann B, Callison E, Barros J, Schultz MP, Tuteja A, Perlin M, Ceccio SL (2021) Turbulent skin friction reduction through the application of superhydrophobic coatings to a towed submerged SUBOFF body. Journal of Ship Research 65(03): 266-274. Doi: 10.5957/JOSR.10190060

Guo BF, Wang YJ, Cao CF, Qu ZH, Song J, Li SN, Gao JF, Song P, Zhang GD, Shi YQ, Tang LC (2024) Large-scale, mechanically robust, solvent-resistant, and antioxidant mXene-based composites for reliable long-term infrared stealth. Advanced Science 11(17): 2309392. https://doi.org/10.1002/advs.202309392

Guo KY, Wu Q, Mao M, Chen H, Zhang GD, Zhao L, Gao JF, Song P, Tang LC (2020) Water-based hybrid coatings toward mechanically flexible, super-hydrophobic and flame-retardant polyurethane foam nanocomposites with high-efficiency and reliable fire alarm response. Composites Part B: Engineering 193: 108017. https://doi.org/10.1016/j.compositesb.2020.108017

Heo S, Choi W, Lee SJ (2021) Enhanced air stability of ridged superhydrophobic surface with nanostructure. AIP Advances 11(10): 105209. DOI: 10.1063/5.0067279

Hosseini H, Mousavi SM (2021) Bacterial cellulose/polyaniline nanocomposite aerogels as novel bioadsorbents for removal of hexavalent chromium: Experimental and simulation study. Journal of Cleaner Production 278: 123817. https://doi.org/10.1016/j.jclepro.2020.123817

Karthik R, Meenakshi S (2015) Removal of Cr (VI) ions by adsorption onto sodium alginate-polyaniline nanofibers. International Journal of Biological Macromolecules 72: 711-717. https://doi.org/10.1016/j.ijbiomac.2014.09.023

Khodakarami M, Bagheri M (2021) Recent advances in synthesis and application of polymer nanocomposites for water and wastewater treatment. Journal of Cleaner Production 296: 126404. https://doi.org/10.1016/j.jclepro.2021.126404

Kim HJ, Im S, Kim JC, Hong WG, Shin K, Jeong HY, Hong YJ (2017) Phytic acid doped polyaniline nanofibers for enhanced aqueous copper (II) adsorption capability. ACS Sustainable Chemistry & Engineering 5(8): 6654-6664. DOI: 10.1021/acssuschemeng.7b00898

Kukkar D, Rani A, Kumar V, Younis SA, Zhang M, Lee SS, Tsang DCW, Kim KH (2020) Recent advances in carbon nanotube sponge–based sorption technologies for mitigation of marine oil spills. Journal of Colloid and Interface Science 570: 411-422. https://doi.org/10.1016/j.jcis.2020.03.006

Liravi M, Pakzad H, Moosavi A, Nouri-Borujerdi A (2020) A comprehensive review on recent advances in superhydrophobic surfaces and their applications for drag reduction. Progress in Organic Coatings 140: 105537. https://doi.org/10.1016/j. porgcoat.2019.105537

Lü X, Cui Z, Wei W, Xie J, Jiang L, Huang J, Liu J (2016) Constructing polyurethane sponge modified with silica/graphene oxide nanohybrids as a ternary sorbent. Chemical Engineering Journal 284: 478-486. https://doi.org/10.1016/j.cej.2015.09.002

Lv XS, Qin Y, Liang H, Zhao B, He Y, Cui X (2021) A facile method for constructing a superhydrophobic zinc coating on a steel surface with anti-corrosion and drag-reduction properties. Applied Surface Science 562: 150192. https://doi.org/10.1016/j.apsusc.2021.150192

Mao M, Yu KX, Cao CF, Gong LX, Zhang GD, Zhao L, Song P, Gao JF, Tang LC (2022) Facile and green fabrication of flame-retardant Ti3C2Tx MXene networks for ultrafast, reusable and weather-resistant fire warning. Chemical Engineering Journal 427: 131615. https://doi.org/10.1016/j.cej.2021.131615

Mendieta-Rodríguez LS, González-Rodríguez LM, Alcaraz-Espinoza JJ, Chávez-Guajardo AE, Medina-Llamas JC (2021) Synthesis and characterization of a polyurethane-polyaniline macroporous foam material for methyl orange removal in aqueous media. Materials Today Communications 26: 102155. https://doi.org/10.1016/j.mtcomm.2021.102155

Mirnezami SA, Zahedi A, Shayan Nejad A (2020) Thermal optimization of a novel solar/hydro/biomass hybrid renewable system for production of low-cost, high-yield, and environmental-friendly biodiesel. Energy 202: 117562. https://doi.org/10.1016/j. energy.2020.117562

Nie F, Gu YL, Zhao L, Li LT, Shen FX, Song J, Liu J, Zhang GD, Gao JF, Song P, Shi Y, Tang LC (2024) Construction of conductive polymer coatings onto flexible PDMS foam composites with exceptional mechanical robustness for sensitive strain sensing applications. Advanced Sensor Research 3(4): 2300140. https://doi.org/10.1002/adsr.202300140

Pan LQ, Zheng QN, Feng QH, Shen YB, Hu WY, Cao CF, Zhang GD, Gao JF, Song P, Shi YQ, Tang LC (2025) Hydrophobic silicone modified membranes for efficient oil/water separation: Synthesis, fabrication and application. Separation and Purification Technology 353: 128485. https://doi.org/10.1016/j.seppur.2024.128485

Qu YX, Xia QQ, Li LT, Cao CF, Zhang GD, Castignolles P, Bae J, Song P, Gao JF, Tang LC (2024) Rational design of oil-resistant and electrically conductive fluorosilicone rubber foam nanocomposites for sensitive detectability in complex solvent environments. ACS Nano 18(33): 22021-22033. DOI: 10.1021/acsnano.4c04135

Sarbatly R, Krishnaiah D, Kamin Z (2016) A review of polymer nanofibres by electrospinning and their application in oil–water separation for cleaning up marine oil spills. Marine Pollution Bulletin 106(1): 8-16. https://doi.org/10.1016/j.marpolbul.2016.03.037

Shen FX, Li Y, Chen ZY, Cao CF, Shen YB, Li LT, Pan LQ, Li JY, Zhang GD, Gao J, Shi Y, Song P, Bae J, Tang LC (2024) Lightweight, surface hydrophobic and flame-retardant polydimethylsiloxane foam composites coated with graphene oxide via interface engineering. Progress in Organic Coatings 189: 108276. https://doi.org/10.1016/j.porgcoat.2024.108276

Singh S, Jelinek R (2020) Solar-mediated oil-spill cleanup by a carbon dot-polyurethane sponge. Carbon 160: 196-203. https://doi.org/10.1016/j.carbon.2020.01.016

Tamsilian Y, Ansari-Asl Z, Maghsoudian A, Abadshapoori AK, Agirre A, Tomovska R (2021) Superhydrophobic ZIF8/PDMS-coated polyurethane nanocomposite sponge: Synthesis, characterization and evaluation of organic pollutants continuous separation. Journal of the Taiwan Institute of Chemical Engineers 125: 204-214. https://doi.org/10.1016/j.jtice.2021.06.023

Tian G, Zhang Y, Feng X, Hu Y (2022) Focus on bioinspired textured surfaces toward fluid drag reduction: recent progresses and challenges. Advanced Engineering Materials 24(1): 2100696. https://doi.org/10.1002/adem.202100696

Turan K, Kaur P, Verma G (2021) Synthesis of conductive polyaniline-carbon nanofiber nanocomposite with chenille like morphology for photocatalytic coatings applications. Progress in Organic Coatings 151: 106102. https://doi.org/10.1016/j.porgcoat.2020.106102

Wu YY, Wu ZH, Chen ZY, Peng LD, Guan ZQ, Li Y, Cao CF, Zhang GD, Gao JF, Song P, Shi YQ, Tang LC (2024) Large-scale and facile fabrication of phenyl-containing silicone foam materials with lightweight, wide-temperature flexibility and tunable pore structure for exceptional thermal insulation. Chemical Engineering Journal 492: 152183. https://doi.org/10.1016/j.cej. 2024.152183

Wu ZH, Feng XL, Qu YX, Gong LX, Cao K, Zhang GD, Shi Y, Gao JF, Song P, Tang LC (2023) Silane modified MXene/polybenzazole nanocomposite aerogels with exceptional surface hydrophobicity, flame retardance and thermal insulation. Composites Communications 37: 101402. https://doi.org/10.1016/j.coco.2022.101402

Xiong S, Yang N, Zhang X, Wang R, Lu Y, Li H, Liu J, Li S, Qiu Z, Wu B, Chu J, Wang X, Zhang R, Gong M, Chen Z (2019) Simultaneous preparation of polyaniline nanofibers/manganese dioxide composites at the interface of oil/water for supercapacitive application. Journal of Electronic Materials 48(10): 6666-6674. DOI: 10.1007/s11664-019-07469-z

Yin H, Zhao J, Li Y, Huang L, Zhang H, Chen L (2020) A novel Pd decorated polydopamine-SiO_2/PVA electrospun nanofiber membrane for highly efficient degradation of organic dyes and removal of organic chemicals and oils. Journal of Cleaner Production 275: 122937. https://doi.org/10.1016/j.jclepro.2020.122937

Zhang GD, Wu ZH, Xia QQ, Qu YX, Pan HT, Hu WJ, Zhao L, Cao K, Chen EY, Yuan Z, Gao JF, Mai YW, Tang LC (2021) Ultrafast flame-induced pyrolysis of poly(dimethylsiloxane) foam materials toward exceptional superhydrophobic surfaces and reliable mechanical robustness. ACS Applied Materials & Interfaces 13(19): 23161-23172. DOI: 10.1021/acsami.1c03272

Zhu H, Qiu S, Jiang W, Wu D, Zhang C (2011) Evaluation of electrospun polyvinyl chloride/polystyrene fibers as sorbent materials for oil spill cleanup. Environmental Science & Technology 45(10): 4527-4531. DOI: 10.1021/es2002343